



This is a repository copy of *Evaluation of in-vivo measurement errors associated with micro-computed tomography scans by means of the bone surface distance approach.*

White Rose Research Online URL for this paper:
<http://eprints.whiterose.ac.uk/90934/>

Version: Accepted Version

Article:

Lu, Y., Boudiffa, M., Dall'Ara, E. et al. (2 more authors) (2015) Evaluation of in-vivo measurement errors associated with micro-computed tomography scans by means of the bone surface distance approach. *Medical Engineering and Physics*. ISSN 1350-4533

<https://doi.org/10.1016/j.medengphy.2015.08.017>

Article available under the terms of the CC-BY-NC-ND licence
(<https://creativecommons.org/licenses/by-nc-nd/4.0/>)

Reuse

Unless indicated otherwise, fulltext items are protected by copyright with all rights reserved. The copyright exception in section 29 of the Copyright, Designs and Patents Act 1988 allows the making of a single copy solely for the purpose of non-commercial research or private study within the limits of fair dealing. The publisher or other rights-holder may allow further reproduction and re-use of this version - refer to the White Rose Research Online record for this item. Where records identify the publisher as the copyright holder, users can verify any specific terms of use on the publisher's website.

Takedown

If you consider content in White Rose Research Online to be in breach of UK law, please notify us by emailing eprints@whiterose.ac.uk including the URL of the record and the reason for the withdrawal request.



eprints@whiterose.ac.uk
<https://eprints.whiterose.ac.uk/>

Medical Engineering and Physics – Technical Note:

About the in vivo micro-computed tomography measurement errors evaluated by the bone surface distance approach

Yongtao Lu^{1,*}, Maya Boudiffa^{2,3,*}, Enrico Dall'Ara¹, Ilaria Bellantuono^{2,3}, Marco Viceconti¹

¹Department of Mechanical Engineering and INSIGNEO Institute for in silico Medicine, the University of Sheffield, Sheffield, UK

²Bone Biology Unit, Department of Human Metabolism and INSIGNEO Institute for in silico Medicine, the University of Sheffield, Sheffield, UK

³MRC-Arthritis Research UK Centre for Integrated Research into Musculoskeletal Ageing (CIMA), UK

*the first two authors share the first authorship

Corresponding author:

Yongtao Lu, Ph.D

INSIGNEO Institute for in silico Medicine and Department of Mechanical Engineering, the University of Sheffield

The Pam Liversidge Building

The Sir Frederick Mappin Building

Mappin Street, S1 3JD, Sheffield, UK

Email: yongtao.lu@sheffield.ac.uk, bennett2001@gmail.com

Tel: +44(0) 114 222 6174

Word count (Introduction through Discussion): 2956

Abstract

In vivo micro-computed tomography (μ CT) scanning is an important tool for longitudinal monitoring of the bone adaptation process in animal models. However, the errors associated with the usage of in vivo μ CT measurements for the evaluation of bone adaptations remain unclear. The aim of this study was to evaluate the measurement errors using the bone surface distance approach. The right tibiae of eight 14-week-old C57BL/6J female mice were consecutively scanned four times in an in vivo μ CT scanner using a nominal isotropic image voxel size ($10.4 \mu\text{m}$) and the tibiae were repositioned between each scan. The repeated scan image datasets were aligned to the corresponding baseline (first) scan image dataset using rigid registration and a region of interest was selected in the proximal tibia metaphysis for analysis. The bone surface distances between the repeated and the baseline scan datasets were evaluated. It was found that the average (\pm standard deviation) median and 95th percentile bone surface distances were $3.10 \pm 0.76 \mu\text{m}$ and $9.58 \pm 1.70 \mu\text{m}$, respectively. This study indicated that there were inevitable errors associated with the in vivo μ CT measurements of bone microarchitecture and these errors should be taken into account for a better interpretation of bone adaptations measured with in vivo μ CT.

Keywords: in vivo μ CT, bone adaptation, bone surface distance, mouse tibia, repeated scans

1. Introduction

Several musculoskeletal pathologies (e.g. osteoporosis) affect the morphology and density of the bone over time, impairing the length and quality of life of the ageing populations through increased frequency of fracture. A number of subject specific modelling approaches have been developed to study the effect of pathologies and drug treatments on the mechanical properties of bone structure [1 - 3]. However, validation of such models is not trivial, because the adaptations of bone density and morphology need to be quantified experimentally over time [4, 5]. Due to the limitation of image resolution in the standard clinical quantitative computed tomography (QCT) scanner, the QCT scanning does not allow the assessment of bone microstructure. The high-resolution peripheral QCT scanning allows the *in vivo* assessment of bone microstructure in human subjects [6], but the scanning region is limited to the human distal tibia and distal radius. Furthermore, it is very difficult to carry out medic interventions in patients. Small rodents, on the other hands, offer a cost-effective and efficient way to speed up the research and development of drug therapies. In addition, the *in vivo* high resolution micro-computed tomography (μ CT) scanning can be performed repeatedly on the complete tibia of small rodents in preclinical studies in order to estimate the adaptations of bone density and microarchitecture over time, often on the same bone of the same animal [7].

In order to quantify bone adaptations in a longitudinal animal study using μ CT, three-dimensional (3D) bone morphometric measurements (trabecular

thickness, trabecular number, trabecular separation, cortex thickness, etc.) over a volume of interest (VOI) (mouse tibia, caudal vertebra and rat tibia, etc.) were used [8 - 11]. However, these morphometric measurements were averaged over the complete bone VOI and therefore cannot provide 3D spatial information of bone adaptations. In order to visualise bone adaptations in 3D, the in vivo μ CT images obtained at the same anatomical site (of the same animal) over different time points need to be superimposed (registered). The following rules were applied when interpreting the superimposed longitudinal image datasets: (a) the newly appeared bone voxels were defined as the formed bone region, (b) the disappeared bone voxels were defined as the resorbed bone region, and (c) the bone voxels present at both time points were defined as quiescent bone region. However, the errors associated with the in vivo μ CT measurement of bone microarchitecture were frequently ignored when using the above rules to interpret bone adaptations [7, 8, 11, 12], which may result in an inaccurate interpretation.

While the highly reproducible bone morphometric measurements do not necessarily imply a high degree of resemblance between two objects, the bone surface distance quantifications (the median distance, the 95% percentile distance, etc.) provide the solution to quantify the degree of resemblance between two superimposed objects [13]. Thereafter, a better interpretation of bone adaptations in the superimposed longitudinal image datasets can be achieved by taking into account the measurement errors assessed by the bone surface distance approach.

The aim of this study was to use the bone surface distance approach to evaluate the experimental errors associated with the *in vivo* μ CT measurements of bone microarchitecture in mouse tibias.

2. Materials and methods

2.1. Animals

Eight 14-week-old female C57BL/6J (BL6) mice were purchased from Harlan Laboratories (Bicester, UK). Prior to the experiment, the mice were allowed to acclimate to the new environment for one week, and were housed in the same environmentally controlled conditions with a twelve-hour light/dark cycle at 22°C and had free access to food and water. All the procedures were complied with the UK Animals (Scientific Procedures) Act 1986 and were reviewed and approved by the local Research Ethics Committee of the University of Sheffield (Sheffield, UK).

2.2. In vivo μ CT scanning

For the duration of *in vivo* μ CT scanning, the mice were placed on a heating pad to keep them warm, maintained under anaesthetic gases (isoflurane) and the complete right tibia of each mouse was scanned four times consecutively using vivaCT 80 (Scanco Medical, Bruettisellen, Switzerland) (approximately four hours per four consecutive scans). Between each scan, the mouse was not woken up but was repositioned in the sample holder to simulate a longitudinal study design. The tibia was firmly fixed in the sample holder with beaded plastic cable

ties (Cable Ties Direct, Sheffield, UK) to prevent any movement during the scan. The scanner was operated at 55 keV, 145 μ A, an integration time of 200 ms and a nominal isotropic image voxel size of 10.4 μ m. The radiation dose from the μ CT scanning was estimated to be approximately 500 mGy for each scan, which has been proved to cause no significant effect on bone adaptations [14]. μ CT is able to characterize the bone mineralization, but it is subject to beam hardening artefacts due to the polychromatic X-ray beam [15]. Therefore, a third-order polynomial beam hardening correction algorithm provided by the manufacturer (Scanco Medical AG), determined using the 1200 mg HA/cm³ wedge phantom, was applied to all the scans [15].

2.3. Image processing

In the image processing chain (**Fig. 1**), first, in order to facilitate the cropping of the baseline images (**Fig. 1a**), the long axis of the mouse tibia from the baseline (first) scan was roughly aligned to the Z-axis in the global coordinate system (Amira 5.4.3, FEI Visualization Sciences Group, France). After rotation and translation, the baseline images were resampled to generate a new image dataset (**Fig. 1b**). To reduce the errors associating with the resampling process, the Lanczos kernel, a low-pass filter (defined by a sinc function) considered to be the ‘best compromise’ among several simple filters [16], was applied to resample the transformed baseline images. After the resampling, part of proximal fibula, the distal femur, and the proximal calcaneus were removed from the images by

cropping the transformed image dataset (**Fig. 1b**) into a smaller dataset which only contained the tibia (**Fig. 1c**). Due to the potential relative movements of the bone segments between repeated scans, the inclusion of proximal fibula, distal femur and proximal calcaneus could potentially influence the outcomes of the subsequent image registration. Afterwards, in order to enable the analysis of the same VOI, the repeated scan image datasets (**Fig. 1d**) were registered to their corresponding baseline scan image dataset (fixed in the registration process) by applying a 3D rigid registration algorithm (Amira 5.4.3), in which the least squares difference of intensities between the baseline scan and a repeated scan image dataset was minimized [17]. To reduce the risk of converging at a local minimum, the rigid registration algorithm consisted of a pyramid strategy, starting at a coarse resampling of the dataset and proceeding to finer resolutions. The registration was performed from the coarsest voxel size until the finest voxel size and stopped when the finest voxel size (10.4 μm) was reached and the convergent criterion (tolerance = 0.0001) of the least squares algorithm was met. Any obvious registration failure (local minimum) was monitored through visual inspections, and registration was performed again until no obvious registration failure. After registration, the Lanczos approximation was applied to resample the registered repeated scan images (**Fig. 1e**). After resampling, the newly generated repeated scan and baseline images shared the same coordinate system, and then the same VOIs were cropped out (**Fig. 1e**). The VOI was set to be the proximal tibia metaphysis, extending 1.31mm distally from the growth plate and

starting at the point where the growth plate tissue was no longer visible in the grayscale CT slices [18]. The grayscale VOI datasets were smoothed with a Gaussian filter (sigma = 1.2, support = 2.0) and binarized into bone and background using a fixed single level threshold, i.e. 25.5% of maximal grayscale value [18]. The applied image threshold values were equivalent to an average (\pm standard deviation) bone mineral density (BMD) of 423 ± 11 mg HA/cm³ (range from 405 mg HA/cm³ to 444 mg HA/cm³) and corresponded to the valley region between the two peaks in the BMD histograms. All the segmentations were checked visually to ensure the proper application of the chosen threshold values. The bone surfaces were reconstructed from the binary image datasets without any smoothing, i.e. the reconstructed surfaces were the outer surfaces of the boundary bone voxels. On average, 391071 ± 119732 (mean \pm standard deviation) surfaces and 197026 ± 60215 vertices were generated to represent each bone VOI. For each mouse, the three repeated scan images were superimposed to the baseline (first) scan images and three evaluation groups were formed. In each group, the bone surface distance at each surface vertex was evaluated (Amira 5.4.3) and the bone surface distance at each surface vertex was defined as the distance from this vertex to the nearest point located at the superimposed bone VOI.

The reproducibility of the bone morphometric measurements and the bone density measurements was analysed in order to compare with the published data. For this purpose, the original grayscale image datasets of the tibia VOI were imported back to the manufacturer (Scanco Medical AG) software and the

cortical and trabecular regions were separated using an automated contouring method [19]. The imported grayscale images were then smoothed using a Gaussian filter (sigma = 1.2, support = 2.0) and binarized into bone and background using 25.5% of the maximum grayscale value as the threshold [18]. Subsequently, the binary images were analysed (Image Processing Language, Scanco Medical, Bruettisellen, Switzerland) to determine the bone morphometric measurements (BV/TV: bone volume fraction, Tb.Th: trabecular thickness, Tb.Sp: trabecular separation, Tb.N: trabecular number and Ct.Th: cortex thickness) and the density measurements (BMD: bone mineral density and TMD: bone mineral content divided by the bone volume).

2.4. Statistical analysis

The normal distribution of the distance data was judged through visual inspections on the histogram plots.

The reproducibility of the morphometric measurements and bone density measurements was characterized by the precision errors (PEs) [20], which were expressed both as absolute values of the standard deviation (SD) (PE_{SD}) and as coefficients of variation (CV) ($PE_{\%CV}$).

$$PE_{SD} = \sqrt{\sum_{j=1}^m SD_j^2 / m} \quad (1)$$

$$PE_{\%CV} = \sqrt{\sum_{j=1}^m \%CV_j^2 / m} \quad (2)$$

with

$$\%CV_j = \frac{SD_j}{\bar{x}_j} \times 100\% \quad (3)$$

where, m is the subject number ($m = 8$ in the current study) and \bar{x}_j is the mean of all x_{ij} for subject j .

To determine how accurate the PEs were, the confidence intervals (CIs) were determined for each of the $PE_{\%CV}$ values using a chi-squared distribution (χ^2).

$$\frac{df}{\chi^2_{1-\frac{\alpha}{2}, df}} PE_{\%CV}^2 < \sigma^2 < \frac{df}{\chi^2_{\frac{\alpha}{2}, df}} PE_{\%CV}^2 \quad (4)$$

where, df is the total degrees of freedom ($df = 24$ in the current study).

The intraclass correlation coefficients (ICCs) were also calculated to quantitatively measure the reproducibility of the datasets [21]. The ICC is the ratio of the inter-subject variance divided by the population variance.

$$ICC = \frac{F_0 - 1}{F_0 + (n - 1)} \quad (5)$$

where, F_0 is the ratio of between-subject mean squares over the residual within-subject mean squares and n is the number of repetitions ($n = 4$ in this study). The values of ICC vary between 0 and 1, where 1 denotes a perfect reproducibility.

More detailed descriptions about the definition of PE_{SD} , $PE_{\%CV}$, CIs and ICCs can be found in Kohler et al. [22] and Nishiyama et al. [10].

3. Results

The bone surface distances in each evaluation group were not normally distributed. Therefore, the 25th, 50th, 75th and 95th percentile distances in each

group were reported (**Table 1 and Fig. 2**). The average (\pm SD) median and 95th percentile distances for the eight mice were $3.10 \pm 0.76 \mu\text{m}$ and $9.58 \pm 1.70 \mu\text{m}$, respectively. In all groups, $95.74 \pm 3.08\%$ (range from 84.38% to 99.79%) of the distances was shorter than $10 \mu\text{m}$ and $0.31 \pm 0.25\%$ (range from 0.01% to 1.29%) of the distances was longer than $20 \mu\text{m}$. The average (\pm SD) maximum distance in all groups was $171.63 \pm 61.84 \mu\text{m}$ (range from $73.59 \mu\text{m}$ to $302.44 \mu\text{m}$). A representative visualisation of the distribution of the bone surface distances in the mouse tibia VOI is shown in **Fig. 3**, which indicated that the distances were shorter than $10 \mu\text{m}$ in most bone surface regions (95.41%), and longer than $20 \mu\text{m}$ only in a few regions (0.09%) with a maximum distance of $153.23 \mu\text{m}$.

The mean morphometric measurements, the bone density measurements, the precision errors (PE_{SD} , $PE_{\%CV}$ and $CI_{95\%}$) and the intraclass correlation coefficients (ICCs) of the measurements are reported in **Table 2**. The precision error $PE_{\%CV}$ ranged from 0.88% (Tb.Th) to 3.93% (Tb.Sp) and the ICCs ranged from 0.893 (TMD) to 0.995 (Ct.Th), which indicated a high reproducibility of the morphometric measurements and the bone density measurements.

4. Discussion

In this study, eight mouse tibias were consecutively scanned four times using the in vivo μCT scanner and the errors associated with the 3D in vivo μCT measurement of the bone microarchitecture were evaluated using the bone surface distance approach. It was found that there were inevitable errors

associated with the in vivo μ CT measurements and for the proximal tibia regions analysed, the average (\pm SD) median and 95th percentile bone surface distances were $3.10 \pm 0.76 \mu\text{m}$ and $9.58 \pm 1.70 \mu\text{m}$, respectively.

Knowing the errors associated with the in vivo μ CT measurement of bone microarchitecture is a prerequisite for an accurate interpretation of bone adaptations in the superimposed longitudinal scan image datasets. For an illustration, the complete tibia of one mouse (BL6) was scanned at the ages of week 14 and week 18 using the scan protocol described in the current study. After superimposing the two image datasets and the application of Boolean operations, four regions should be defined for a better interpretation of bone adaptation: (a) an unclear region, the size of which is determined by the measurement error; (b) a bone formation region, formed by the newly appeared bone voxels; (c) a bone resorption region, formed by the disappeared bone voxels; and (d) a quiescent bone region, formed by the bone voxels present at both time points (**Fig. 4**). In this study, for the proximal tibia regions analysed, the average (\pm SD) median and 95th percentile surface distances were small, i.e. $3.10 \pm 0.76 \mu\text{m}$ and $9.58 \pm 1.70 \mu\text{m}$, respectively, which means that the reconstructed bone surfaces in each group highly resembled each other. However, in a few regions ($0.31\% \pm 0.25\%$), the bone surface distances were longer than $20 \mu\text{m}$ (**Fig.3**), which could be due to the discrepancies in these reconstructed regions caused by thin trabeculae, the noise in the image datasets, or the image processing methods (registration, transformation, segmentation, etc.).

The reproducibility of the morphometric measurements has been previously evaluated in a few studies [10, 11, 22]. Among them, one study [10] was comparable to the current work by the study set-up (analysis region, scan protocol). Similar reproducibility results were found, i.e. for all the parameters analysed, the absolute difference of $PE_{\%cv}$ ranged from 0.24% (TMD) to 1.46% (Tb.N) and those of ICC ranged from 0.028 (Tb.N) to 0.319 (TMD) (**Table 2**). The small differences might be due to the discrepancy in the image processing methods. While the optimization measure of mutual information and the linear interpolation was applied in Nishiyama et al. [10], the Euclidean optimization measure and the Lanczos interpolation were used in this article.

In this study, a couple of points need to be noted. First, the measurement errors obtained in this study can be considered as the lower bound among the values generated from other interpolation methods. This is due to the application of the Lanczos interpolation kernel, which produces the results comparable to the B-spline kernel [23] and the lowest interpolation error compared to other interpolation methods (i.e. the nearest neighbour and tri-linear interpolations) [24]. Second, even though the values of the in vivo μ CT measurement errors depend on the μ CT scanner, the scan protocol, the image processing methods, etc., the current study proposed a methodology, i.e. the bone surface distance method, to estimate the in vivo μ CT measurement errors.

On the other hand, some limitations should be noted in this study. First, the first scan of each mouse was considered as the baseline scan and as the reference

for the comparisons. The comparisons between the repeated scans were not made. Nevertheless, the inevitable errors associated with the in vivo μ CT measurements were found. Second, bone surfaces with jagged edges were generated, because no smoothing was applied when generating the surfaces from binary images. These jagged edges may contribute to the measurement errors calculated using the bone surface distance approach. Nevertheless, the interpretation of bone adaptation is based on the binary images. Last but not least, the mice were not woken up in the repeated scans, which is a necessary step when the in vivo longitudinal studies are performed. However, it would take a few hours for the mice to recover from anaesthesia and thus to complete the four-time scans with the wake-up procedure between would take around 48 hours, within which period the bone adaptation would have a significant influence on the reproducibility of the bone morphometric parameters [25] and also on the measurement error analysed by the bone surface distance approach. The procedure employed in this study dramatically reduced the effect of bone adaptation by completing the four-time scans of each tibia within four hours. Furthermore, in the designed procedure, the measurement error was evaluated in the in vivo scenario and thus the potential motion artefacts induced by the mouse breathing, which could occur in the longitudinal study, were also accounted for in the analysis.

In conclusion, this study used the bone surface distance approach to evaluate the errors associated with the in vivo μ CT measurement of bone microarchitecture and it was found that the average (\pm SD) median and 95th

percentile bone surface distances were $3.10 \pm 0.76 \mu\text{m}$ and $9.58 \pm 1.70 \mu\text{m}$, respectively, for the proximal tibia analysed. This study implied that for a better visualisation and quantification of bone adaptations, the inevitable measurement errors should be taken into account when interpreting the superimposed 3D longitudinal scan image datasets.

Conflict of interest statement

The authors have no conflicts to declare.

Acknowledgements

This work was funded by the UK National Centre for the Replacement, Refinement and Reduction of Animals in Research (NC3Rs), Grant number: NC/K000780/1. The authors would like to acknowledge Dr. Jafar Alsayednoor for his help in the plot of some figures and Dr. Xinshan Li for the proofreading.

Reference:

1. Christen D, Webster DJ, Mueller R. Multiscale modelling and nonlinear finite element analysis as clinical tools for the assessment of fracture risk. *Philos Trans A Math Phys Eng Sci* 2010; 368(1920): 2653-68.
2. Keaveny TM, Hoffmann PF, Singh M, Palermo L, Bilezikian JP, Greenspan SL, Black DM. Femoral Bone strength and its relation to cortical and trabecular changes after treatment with PTH, Alendronate, and their combination as assessed by finite element analysis of quantitative CT scans. *J Bone Miner Res* 2008; 23(12): 1974-82.
3. Vahdati A, Walscharts S, Jonkers I, Garcia-Aznar JM, Vander Sloten J, van Lenthe GH. Role of subject-specific musculoskeletal loading on the prediction

- of bone density distribution in the proximal femur. *J Mech Behav Biomed Mater* 2014; 30: 244-52.
4. Levchuk A, Zwahlen A, Weigt C, Lambers FM, Badilatti SD, Schulte FA, et al. Large scale simulations of trabecular bone adaptation to loading and treatment. *Clin Biomech* 2014; 29(4): 355 – 62.
 5. Schulte FA, Zwahlen A, Lambers FM, Kuhn G, Ruffoni D, Betts D, et al. Strain-adaptive in silico modelling of bone adaptation – a computer simulation validated by in vivo micro-computed tomography data. *Bone* 2013; 52(1): 485 – 92.
 6. Nishiyama KK, Macdonald HM, Buie HR, Hanley DA, Boyd SK. Postmenopausal women with osteopenia have higher cortical porosity and thinner cortices at the distal radius and tibia than women with normal aBMD: An in vivo HR-pQCT study. *J Bone Miner Res* 2009; 25(4): 882 – 90.
 7. Waarsing J, Day J., van der Linden J, Ederveen A, Spanjers C, De Clerck N, et al. Detecting and tracking local changes in the tibiae of individual rats: a novel method to analyse longitudinal in vivo micro-CT data. *Bone* 2004; 34(1): 163 – 69.
 8. Birkhold AI, Razi H, Duda GN, Weinkamer R, Checa S, Willie BM. The influence of age on adaptive bone formation and bone resorption. *Biomaterials* 2014; 35: 9290-301.
 9. Lambers FM, Koch K, Kuhn G, Ruffoni D, Weigt C, Schulte FA, Mueller R. Trabecular bone adapts to long-term cyclic loading by increasing stiffness and normalization of dynamic morphometric rates. *Bone* 2013; 55(2): 325 – 334.
 10. Nishiyama KK, Campbell GM, Klinck RJ, Boyd SK. Reproducibility of bone micro-architecture measurements in rodents by in vivo micro-computed tomography is maximized with three-dimensional image registration. *Bone* 2010; 46(1): 155 – 61.
 11. Schulte FA, Lambers FM, Kuhn G, Mueller R. In vivo micro-computed tomography allows direct three-dimensional quantification of bone formation

- and bone resorption parameters using time-lapsed imaging. *Bone* 2011; 48(3): 433 – 42.
- 12.Schulte FA, Lambers FM, Webster DJ, Kuhn G, Mueller R. In vivo validation of a computational bone adaptation model using open-loop control and time-lapsed micro-computed tomography. *Bone* 2011; 49(6): 1166-1172.
 - 13.Huttenlocher DP, Klanderman GA, Rucklidge WJ. Comparing images using the Hausdorff distance. *IEEE Trans Pattern Anal Mach Intell* 1993; 15(9): 850 – 63.
 - 14.Laperre K, Depypere M, van Gastel N, Torrekens S, Moermans K, Bogaerts R, et al. Development of micro-CT protocols for in vivo follow-up of mouse bone architecture without major radiation side effects. *Bone* 2011; 49(4): 613-22.
 - 15.Fajardo RJ, Cory E, Patel ND, Nazarian A, Laib A, Manoharan RK, et al. Specimen and Porosity can introduce error into microCT-based tissue mineral density measurements. *Bone* 2009; 29: 2672-81.
 - 16.Turkowski K, Gabriel S. Filters for common resampling tasks. In Glassner AS. *Graphics Gems 1*. Academic Press 1990: 147 – 65.
 - 17.Thevenaz P, Ruttimann UE, Unser M, A pyramid approach to subpixel registration based on intensity. *IEEE Trans Image Process* 1998; 7(1): 27 – 41.
 - 18.Klinck RJ, Campbell GM, Boyd SK. Radiation effects on bone architecture in mice and rats resulting from in vivo micro-computed tomography scanning. *Med Eng Phys* 2008; 30(7): 888 – 95.
 - 19.Buie HR, Campbell GM, Klinck RJ, MacNeil JA, Boyd SK. Automatic segmentation of cortical and trabecular compartments based on a dual threshold technique for in vivo micro-CT bone analysis. *Bone* 2007; 41(4): 505-15.
 - 20.Glueer C, Blake G, Lu Y, Blunt BA, Jergas M, Genant HK. Accurate assessment of precision errors: how to measure the reproducibility of bone densitometry techniques. *Osteoporos Int* 1995; 5(4): 262-70.

21. Shrout P, Fleiss J. Intraclass correlations: uses in assessing rater reliability. *Psychol Bull* 1979; 86(2): 420 – 28.
22. Kohler T, Beyeler M, Webster D, Mueller R. Compartmental bone morphometry in the mouse femur: reproducibility and resolution dependence of microtomographic measurements. *Calcif Tissue Int* 2005; 77(5): 281- 90.
23. Meijering EHW. Spline interpolation in medical imaging: comparison with other convolution-based approaches. In: Gabbouj, Kuosmanen, editors. *Signal processing X: theories and applications – proceedings of EUSIPCO 2000, M., the European association for signal processing, Tampere, vol. IV; 2000: 1989-96.*
24. Schulte FA, Lambers FM, Mueller TL, Stauber M, Mueller R. Image interpolation allows accurate quantitative bone morphometry in registered micro-computed tomography scans. *Comput Methods Biomech Biomed Engin* 2014; 17(5): 539 – 48.
25. Glatt V, Canalis E, Stadmeier L, Bouxsein ML. Age-related changes in trabecular architecture differ in female and male C57BL/6J mice. *J Bone Miner Res* 2007; 22(8): 1197-207.

Table 1. The 25th, 50th, 75th and 95th percentile bone surface distances between the three repeated scan datasets and the baseline scan dataset for the eight mouse tibias.

		Bone surface distance [μm]			
		25% percentile	50% percentile	75% percentile	95% percentile
Mouse 1	RS1 .vs. BS*	1.06	1.97	3.56	6.28
	RS2 .vs. BS	0.94	1.94	3.40	5.89
	RS3 .vs. BS	1.18	2.48	4.28	7.15
Mouse 2	RS1 .vs. BS	1.49	2.49	4.91	9.30
	RS2 .vs. BS	1.55	2.77	5.08	9.53
	RS3 .vs. BS	1.88	3.57	6.23	11.16
Mouse 3	RS1 .vs. BS	1.26	3.77	6.17	10.68
	RS2 .vs. BS	2.20	4.25	6.69	12.12
	RS3 .vs. BS	1.96	3.74	6.54	11.44
Mouse 4	RS1 .vs. BS	1.46	2.73	6.03	10.39
	RS2 .vs. BS	1.61	2.32	6.00	9.50
	RS3 .vs. BS	1.83	4.38	5.82	11.16
Mouse 5	RS1 .vs. BS	1.24	2.61	4.76	8.41
	RS2 .vs. BS	1.29	2.57	4.62	7.82
	RS3 .vs. BS	1.31	2.58	4.70	8.15
Mouse 6	RS1 .vs. BS	1.19	2.39	4.38	8.01
	RS2 .vs. BS	1.56	3.23	5.61	9.85
	RS3 .vs. BS	1.61	3.36	5.93	10.52
Mouse 7	RS1 .vs. BS	1.50	3.41	4.99	9.67
	RS2 .vs. BS	1.48	3.08	5.95	9.67
	RS3 .vs. BS	1.87	4.53	6.93	12.00
Mouse 8	RS1 .vs. BS	1.85	2.94	5.89	9.91
	RS2 .vs. BS	1.69	3.12	5.53	10.22
	RS3 .vs. BS	1.96	4.33	6.63	11.14

(* RS: repeated scan; BS: baseline scan)

Table 2. The mean \pm standard deviation (SD) values of all the morphometric and density measurements (eight mice and four scans for each mouse), of the corresponding reproducibility data (PE_{SD}: precision error of SD; PE_{%CV}: precision error of the coefficient of variation; CI_{95%}: 95% confidence interval of PE_{%CV}; ICC: intraclass correlation coefficient) and comparisons with literature.

Parameter	Data from this study					Data from Nishiyama et al. 2010 [10]	
	Mean \pm SD	PE _{SD}	PE _{%Cv} (%)	CI _{95%} (PE _{%CV}) (%)	ICC	PE _{%CV} (%)	ICC
Tb.Th [mm]	0.053 \pm 0.004	0.0005	0.88	0.72 – 1.16	0.986	1.77	0.790
Tb.Sp [mm]	0.473 \pm 0.080	0.0190	3.93	3.19 – 5.17	0.952	2.65	0.904
Tb.N [1/mm]	2.190 \pm 0.360	0.0800	3.61	2.93 - 4.76	0.956	2.15	0.928
Ct.Th [mm]	0.158 \pm 0.013	0.0010	0.65	0.53 – 0.86	0.995	0.95	0.950
BV/TV (%)	4.690 \pm 1.280	1.0600	2.25	1.73 – 2.80	0.994	2.98	0.818
BMD [mgHA/cm³]	398.11 \pm 37.02	7.4800	1.88	1.53 – 2.47	0.963	1.41	0.776
TMD [mgHA/cm³]	987.63 \pm 34.67	11.870	1.20	0.98 – 1.58	0.893	0.96	0.574

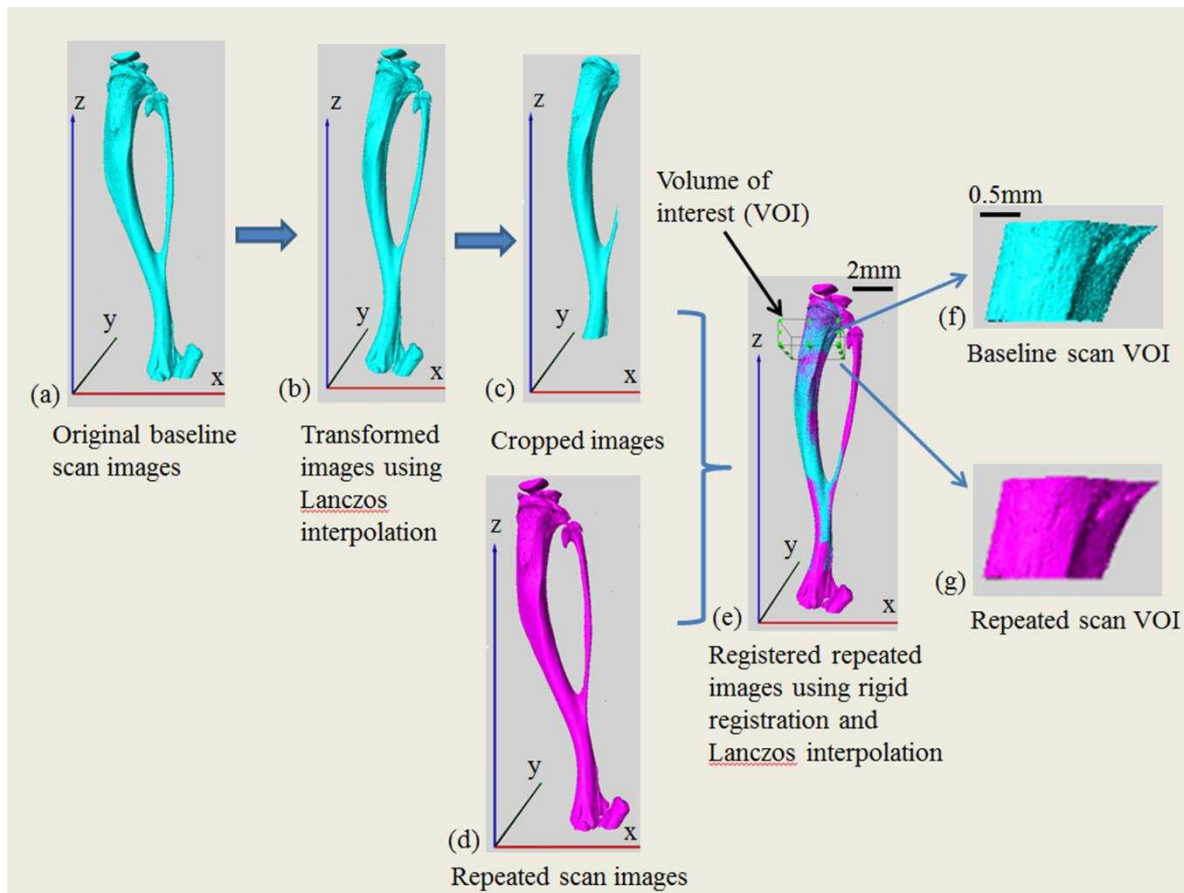


Fig. 1. Overview of the image processing chain; the original baseline scan image (a), the transformed baseline image (b), the cropped baseline image (c), the repeated scan image (d), the registered repeated scan image (e), the volumes of interest for both the baseline (f) and the repeated scan images (g).

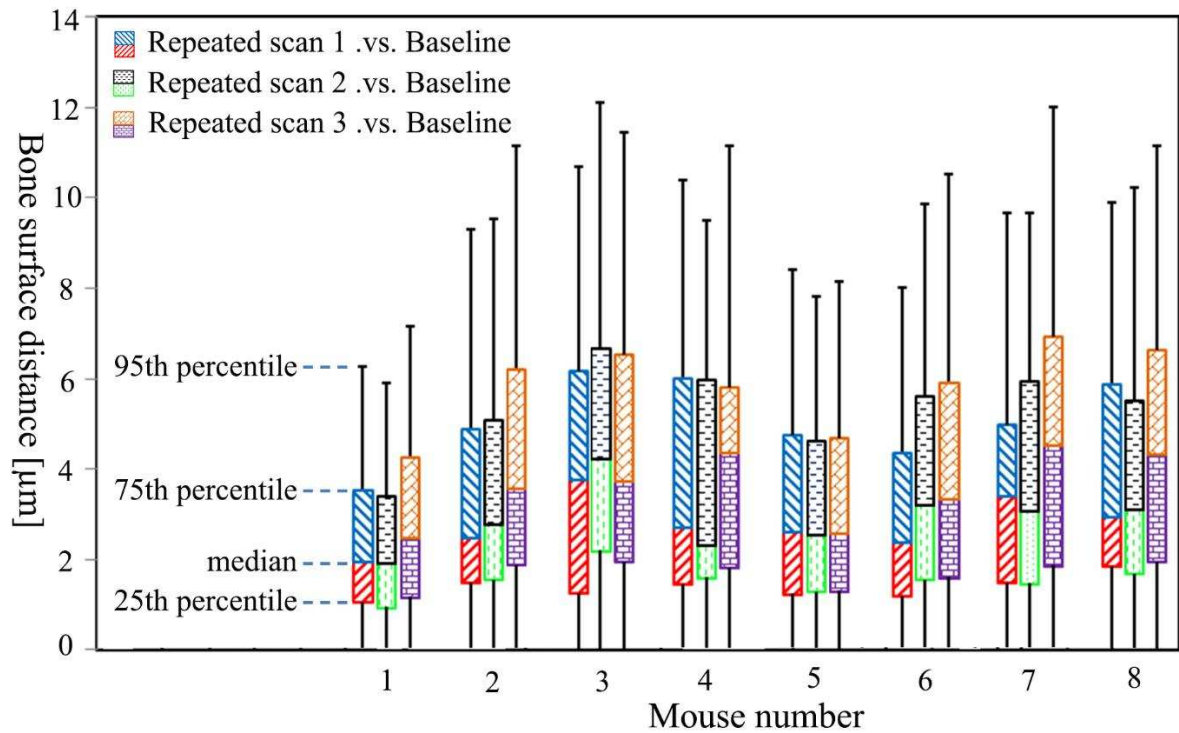


Fig. 2. The 25th, 50th, 75th and 95th percentile bone surface distances between the three repeated scan datasets and the baseline scan dataset for the eight mouse tibias.

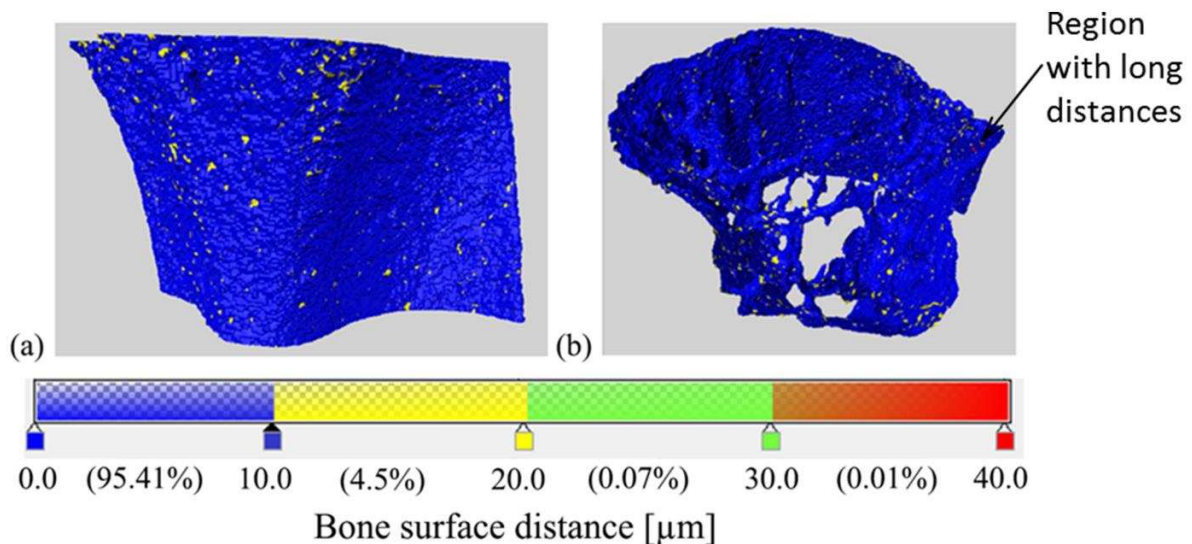


Fig. 3. A representative plot of the distribution of the bone surface distances in the mouse tibia volume of interest; lateral view (a) and proximal-distal view (b)

(the numbers in the parentheses represents the percentage of data falling within the specified distance ranges)

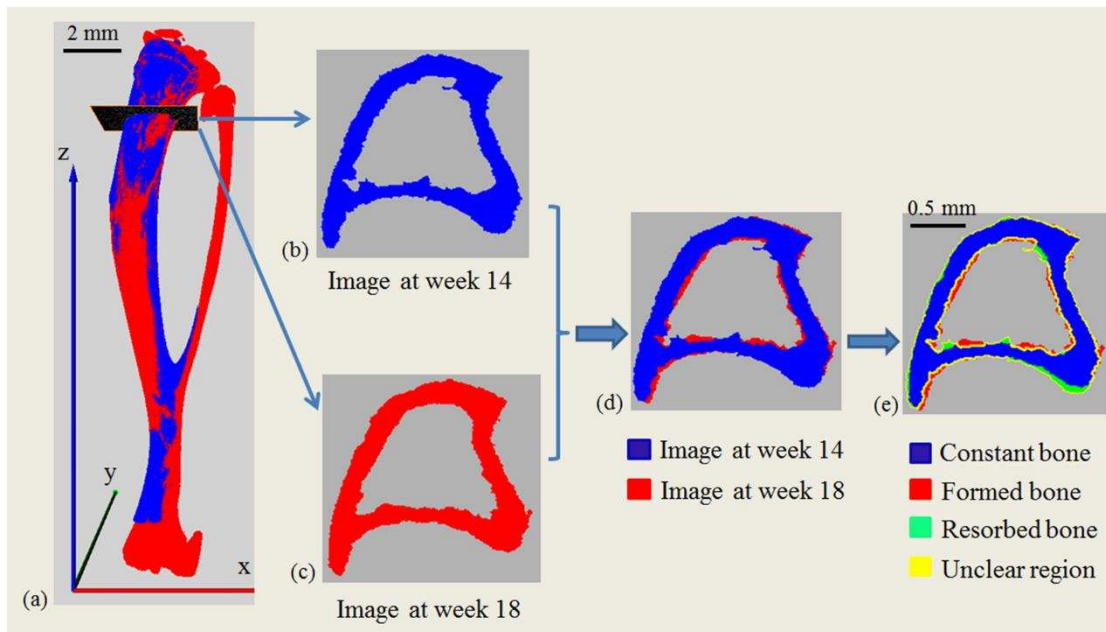


Fig. 4. A representative illustration for interpreting bone adaptations in the mouse tibia images obtained at the ages of weeks 14 and 18; the registered images (a), the cross-sectional images at week 14 (b) and week 18 (c), the superimposed cross-sectional images (d) and the interpretation of bone adaptation considering the measurement error(e).